



# Activation of persulfate with vanadium species for PCBs degradation: A mechanistic study

Guodong Fang<sup>a</sup>, Wenhui Wu<sup>a</sup>, Cun Liu<sup>a</sup>, Dionysios D. Dionysiou<sup>b</sup>, Yamei Deng<sup>a</sup>, Dongmei Zhou<sup>a,\*</sup>

<sup>a</sup> Key Laboratory of Soil Environment and Pollution Remediation, Institute of Soil Science, Chinese Academy of Sciences, Nanjing, 210008, PR China

<sup>b</sup> Environmental Engineering and Science Program, University of Cincinnati, Cincinnati, OH, 45221-0071, USA



## ARTICLE INFO

### Article history:

Received 2 March 2016

Received in revised form 1 September 2016

Accepted 2 September 2016

Available online 3 September 2016

### Keywords:

Persulfate

Vanadium oxides

Activation

PCBs

ISCO

## ABSTRACT

In the present study, the activation of persulfate (PS) with vanadium (V) species for PCBs (2,4,4'-trichlorobiphenyl [PCB28]) degradation was investigated for the first time. It was found that  $V_2O_3$  exhibited high catalytic activity toward PS decomposition for PCB28 degradation. Even under near neutral pH (7.4), PCB28 was efficiently degraded in  $V_2O_3/PS$ . Sulfate radical anions ( $SO_4^{2-}$ ) and hydroxyl radicals ( $\cdot OH$ ) were produced from PS activation with  $V_2O_3$  for PCB28 degradation, and were characterized with electron paramagnetic resonance (EPR) technique. Free radical quenching studies showed that ethanol inhibited PCB28 degradation, while *tert*-butyl alcohol enhanced PCB28 degradation via reductive dechlorination with alcohol radicals. The pathway of PCB28 degradation was proposed on the basis of GC-MS analysis of intermediates of PCB28 degradation in  $V_2O_3/PS$ . The mechanisms of PS activation are elucidated. It was found that V(III) in  $V_2O_3$  activated PS to form  $SO_4^{2-}$  and V(IV) ( $VO_2$ ) via electron transfer process, and the formed V(IV) further transferred an electron to PS to generate  $SO_4^{2-}$  and V(V) ( $V_6O_{13}$ ), which were supported with XRD analysis. Furthermore, both  $VO_2$  and  $V_2O_5$  can activate PS for PCB28 degradation, indicating that V(IV) would be regenerated from the reduction of V(V) by persulfate ions ( $S_2O_8^{2-}$ ) on the surface of  $V_2O_5$  particles. These findings would help to better understand the interactions between naturally occurring V minerals and PS, and provide a novel activator for PS activation to degrade contaminants.

© 2016 Elsevier B.V. All rights reserved.

## 1. Introduction

Persulfate (PS)-based in-situ chemical oxidation (ISCO) for the remediation of contaminated soils and groundwater has attracted great attention in recent years [1–4]. Diverse contaminants including chlorinated compounds, polycyclic aromatic hydrocarbons, polychlorinated biphenyls, and refractory pollutants can be degraded by PS activated with heat, UV light, bases,  $H_2O_2$ , and transition metals; the efficiency of each treatment depends on the contaminant type and subsurface conditions [5–15]. The soil or subsurface components such as naturally occurring minerals and organic matter affect the activation of PS and formation of reactive oxygen species (ROS) that influence the remediation efficiency of contaminated soil. Therefore, the effects of subsurface chemistry on PS activation have been widely investigated [16,17]. For

example, it has been reported that quinones or phenols activate PS efficiently for contaminant degradation [18,19]. Minerals such as magnetite, pyrite, and siderite can also activate PS [20–22]. Thus, naturally occurring minerals play an important role in PS decomposition and contaminant degradation. Most of the previous studies mainly investigated the effects of Fe and Mn-minerals on PS activation and contaminant degradation [23,24]; however, the activation of PS with other minerals such as vanadium species has been rarely investigated.

V accounts for ~0.01% of the total mass of the Earth's crust and is widely distributed in the natural environment and biological systems [25,26]. The concentration of V in soil ranges from trace amounts to 400 mg/kg, with an average of 90 mg/kg, depending on the parent material and occurrence of V-containing ore minerals in the subsoil [27,28]. The prevailing valence states of V in nature are V(III), V(IV), and V(V); the latter two are much more soluble in water [29,30], while V(III) is dominant in reduced conditions with less mobility [31]. Furthermore, V usually coexists with other metal minerals in the soil, for example it has been reported that

\* Corresponding author.

E-mail address: [dmzhou@issas.ac.cn](mailto:dmzhou@issas.ac.cn) (D. Zhou).

about 65 naturally occurring minerals such as carnotite, roscoelite, vanadinite, patronite, bravoite and davidite contain V [29]. Because of industrial activities and anthropogenic emissions, the concentration of V in soil has increased significantly in recent years [32]. Therefore, it is imperative to examine the interactions between V species and PS or the possibility that PS can be activated by V species for contaminant degradation, which would help in developing cost-effective strategies for the remediation of contaminated soil based on PS-ISCO. Naturally occurring V minerals are the best candidates to act as model V species for PS activation. However, V minerals usually contain other metals such as Ti and Fe, which would also contribute to the activation of PS, and thus it is difficult to identify the contributions of different metals for PS activation and elucidate the mechanism of PS activation with V species.

Vanadium oxide is considered to be one of the most important materials used as a catalyst due to its unique physical and chemical properties [33]. Vanadium oxide or supported vanadium oxide catalysts have been used in many industrial catalytic processes [34–36], and numerous catalytic reactions in the chemical, petroleum and environmental industries [37,38]. For example, vanadium oxide deposited on a large surface area oxide support such as  $\text{Al}_2\text{O}_3$ ,  $\text{SiO}_2$ ,  $\text{TiO}_2$ , and  $\text{ZrO}_2$  is an efficient catalyst for the oxidative dehydrogenation of propane to produce propene [39]. Silica-supported vanadium oxide is highly active and used in a variety of oxidation reactions, such as the selective oxidation of methane to formaldehyde, the oxidative dehydrogenation of alkanes, and the selective photo-oxidation of alcohols [40]. However, to the best of our knowledge, catalytic decomposition of oxidants such as PS and hydrogen peroxide with V species for the degradation of organic contaminants in environmental applications has not yet been explored.

Therefore, the main objective of this study was to explore the activation of PS with V species for degradation of organic contaminants.  $\text{V}_2\text{O}_3$  was selected as model V species to activate PS for 2,4,4'-trichlorobiphenyl (PCB28) degradation in heterogeneous reactions.  $\text{V}_2\text{O}_3$  was selected as model V (III) species since V(III) could be converted to V(IV) and V(V) species in the presence of persulfate, which was beneficial for simultaneously elucidating the interaction mechanism of persulfate and different valence of V species in minerals by mathematically separating their kinetic contributions. Gas chromatography mass spectrometry (GC-MS) and EPR techniques were used to elucidate the mechanisms of PCB28 degradation and PS activation in  $\text{V}_2\text{O}_3$ /PS. PCB28 was selected as the target pollutant because PCBs are an important group of persistent pollutants, and can be easily degraded with sulfate radicals and hydroxyl radicals [41,42]. Additionally, PS activation with  $\text{VO}_2$  and  $\text{V}_2\text{O}_5$  for PCB28 degradation was also studied to elucidate the pathways of PS activation by  $\text{V}_2\text{O}_3$ .

## 2. Materials and methods

### 2.1. Chemicals

2,4,4'-trichlorobiphenyl (PCB28) was purchased from AccuStandard (New Haven, CT, UAS); 5,5-dimethyl-1-pyrrolidine *N*-oxide (DMPO, 97%) was supplied by Sigma-Aldrich (Saint Louis, MO, USA). 4-chlorobenzoic acid (4-CBA, 99%), 2,4-dichlorobenzoic acid (2,4-D, purity > 95%), vanadium oxides including  $\text{V}_2\text{O}_3$  (99.99%),  $\text{VO}_2$  (74%  $\text{VO}_2$  and 26%  $\text{V}_6\text{O}_{13}$ ), and  $\text{V}_2\text{O}_5$  (98%) were obtained from J&K Scientific Ltd. (Shanghai, China). Sodium persulfate ( $\text{Na}_2\text{S}_2\text{O}_8$ , 99%), potassium iodide (KI, 99%), and sodium bicarbonate ( $\text{NaHCO}_3$ , 99%) were purchased from China National Medicines Corporation Ltd. (Beijing, China). Deionized water with a resistivity of  $18 \text{ M}\Omega \text{ cm}^{-1}$  was used in the experiments.

### 2.2. Characterization of commercial vanadium oxides

The morphologies of  $\text{V}_2\text{O}_3$ ,  $\text{VO}_2$ , and  $\text{V}_2\text{O}_5$  were determined by scanning electron microscopy (SEM, S3400N II, Hitachi, Japan), and X-ray diffraction (XRD), a Rigaku Dmax-RB-XRD with a Cu  $\text{K}\alpha$  radiation source generated at 40 kV and 20 mA (Figs. S1 and S2). The SEM images showed that  $\text{V}_2\text{O}_3$  is composed of some irregularly spherical particles with size of  $\sim 4 \mu\text{m}$ ,  $\text{VO}_2$  is layered with large size ( $50\text{--}100 \mu\text{m}$ ) and covered by clubbed particles with length of  $\sim 4.2 \mu\text{m}$ , and width of  $\sim 1.0 \mu\text{m}$ , and  $\text{V}_2\text{O}_5$  is clubbed particle with length of  $\sim 4.2 \mu\text{m}$ . Laser diffraction particle size analyzer (Beckman LS13320, USA) was used to further characterize the particle distribution (Table S1). The results suggest that 71.8% of  $\text{V}_2\text{O}_3$  and 57%  $\text{V}_2\text{O}_5$  particles are  $<2 \mu\text{m}$ , while 68.2% of  $\text{VO}_2$  particles are  $<50 \mu\text{m}$ . XRD results show that  $\text{V}_2\text{O}_3$  and  $\text{V}_2\text{O}_5$  were pure, whereas  $\text{VO}_2$  comprised of about 24% of  $\text{V}_6\text{O}_{13}$ , in which V(IV) and V(V) coexisted. It indicates that V(IV) was partially oxidized to V(V) during the synthesis of  $\text{VO}_2$ . The specific surface areas of  $\text{V}_2\text{O}_3$ ,  $\text{VO}_2$ , and  $\text{V}_2\text{O}_5$  were 4.61, 4.67 and  $22.4 \text{ m}^2/\text{g}$ , respectively, determined using the Brunauer–Emmett–Teller nitrogen-adsorption method at 77 K (ASAP 2460, micromeritics, USA).

### 2.3. Degradation experiments

Batch experiments were performed in the dark using 40-mL brown serum bottles sealed with Teflon Mininert containing 20 mL of the reaction mixtures. Different amounts of V oxides were dispersed into an aqueous solution of PCB28 (19 mL) with final concentration of  $3.9 \mu\text{M}$ . After mixing thoroughly, 1.0 mL of 40 mM PS (the final concentration was 2.0 mM) was added, and the mixtures were shaken at 150 rpm, 25 °C, and pH 5.9. All the control experiments were performed using V oxides or PS alone under the same reaction conditions. Periodically, the samples were analyzed after adding 1.0 mL ethanol to quench the reaction. Then, 5.0 mL hexane was used to extract the remaining PCB28 in the quenched reaction mixture. The hexane phase was analyzed by a gas chromatograph (GC, Agilent7890, USA) equipped with a  $\text{Ni}^{63}$  electron-capture detection (ECD) device. To identify the products of PCB28 degradation, the suspension obtained after the reaction was extracted with dichloromethane, derivatized with BSTFA/TCMS (99:1 v/v), and analyzed using a gas chromatography mass spectrometry (GC-MS, QP 2010, Shimadzu, Japan). The concentration of PS was determined by a spectrophotometric method according to a previous study [43]. The total vanadium ion concentration obtained from vanadium oxides was determined using an inductively coupled plasma optical emission spectrometry (ICP-AES, Perkin-Elmer, Optima 8000, USA). The concentration of chloride ion formed from reaction solution was quantified with a DX-500 ion chromatograph (IC, DIONEX Company, Germany). The effects of pH on PCB28 degradation in  $\text{V}_2\text{O}_3$ /PS were conducted under the same reaction conditions except that pH was buffered with borate (pH 7.4 and 8.4, 50 mM borate). All the experiments were carried out in triplicate, and the results were reported as mean with standard deviations. The other analysis methods used in this study are reported in Text S1.

### 2.4. Electron paramagnetic resonance (EPR) studies

The  $\text{SO}_4^{\bullet-}$  and  $\bullet\text{OH}$  generated by PS activation using  $\text{V}_2\text{O}_3$  were identified by EPR using 5,5-dimethyl-1-pyrroline-*N*-oxide (DMPO) as the spin-trapping agent. Different vanadium oxides, PS (2.0 mM), and DMPO (0.1 M) were reacted. The EPR spectra were obtained at room temperature using a Bruker EMX/Plus spectrometer (Germany) with a resonance frequency of 9.77 GHz, microwave power of 19.97 mW, modulation frequency of 100 kHz, modulation amplitude of 1.0 G, sweep width of 100 G, time constant of 40.96 ms,

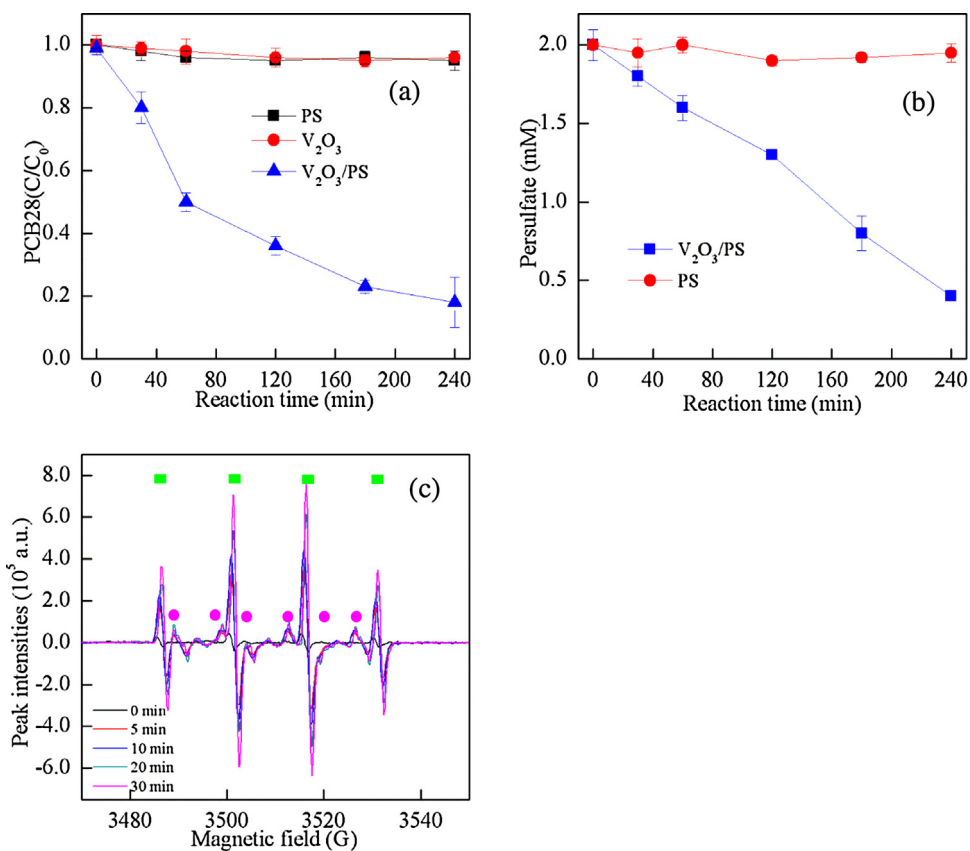


**Fig. 1.** Activation of PS by V<sub>2</sub>O<sub>3</sub> for PCB28 degradation: kinetics of PCB28 degradation (a), and PS decomposition (b) in the V<sub>2</sub>O<sub>3</sub>/PS system; (c) EPR spectra of V<sub>2</sub>O<sub>3</sub>/PS suspension with DMPO as spin-trapping agent. Reaction conditions: [PS]<sub>0</sub> = 2.0 mM; V<sub>2</sub>O<sub>3</sub> loading: 0.05 g/L; [PCB28]<sub>0</sub> = 3.9 μM; [DMPO]<sub>0</sub> = 100 mM; pH 5.9 and 25 °C. Green square: DMPO-OH; pink circle: DMPO-SO<sub>4</sub>. (For interpretation of the references to colour in this figure legend, the reader is referred to the web version of this article.)

sweep time of 83.89 s, and receiver gain of  $2.0 \times 10^4$ . The peak intensities of DMPO-SO<sub>4</sub> and DMPO-OH were used to determine the concentrations of SO<sub>4</sub><sup>•-</sup> and •OH by measuring the height of the main low-field peak (in arbitrary units determined by instrument parameters), corrected for background noise.

### 3. Results and discussion

#### 3.1. Activation of persulfate by V<sub>2</sub>O<sub>3</sub> for PCB28 degradation

##### 3.1.1. Kinetics of PCB28 degradation and free radical identification

The activation of PS by V<sub>2</sub>O<sub>3</sub> for PCB28 degradation was examined. As shown in Fig. 1a, 82% of PCB28 (3.9 μM) was degraded within 240 min by PS (2.0 mM) in the presence of 0.05 g/L V<sub>2</sub>O<sub>3</sub> at pH 5.9 initially (without buffer), while <10% of PCB28 was degraded when a suspension of V<sub>2</sub>O<sub>3</sub> or solution of PS was used alone. PS concentration was also determined during the degradation of PCB28 in V<sub>2</sub>O<sub>3</sub>/PS, since SO<sub>4</sub><sup>•-</sup> and •OH are usually generated by PS decomposition in a PS activation system, and a decrease in PS concentration is often used as a proxy for radical production.<sup>21</sup> As shown in Fig. 1b, the PS concentration decreased rapidly from 2.0 to 0.4 mM in 240 min, while changed insignificantly ( $p > 0.05$ ) in the solution without V<sub>2</sub>O<sub>3</sub>. These results indicate that PS can be activated by V<sub>2</sub>O<sub>3</sub> for PCB28 degradation.

It has been reported that SO<sub>4</sub><sup>•-</sup> is produced when PS is activated, and SO<sub>4</sub><sup>•-</sup> can further react with H<sub>2</sub>O or •OH to form •OH [44]. Both SO<sub>4</sub><sup>•-</sup> and •OH are responsible for contaminant degradation [44]. Therefore, the free radicals generated in the PS/V<sub>2</sub>O<sub>3</sub> system were further identified by EPR using DMPO as the spin-trapping agent. As shown in Fig. 1c, DMPO-SO<sub>4</sub> (six lines, 1:1:1:1:1:1) and DMPO-

OH (four lines, 1:2:2:1) signals can be attributed to the formation of SO<sub>4</sub><sup>•-</sup> and •OH, respectively, as reported in our previous study [45]. The hyperfine splitting constants were as follows:  $a_H = a_N = 14.9$  G for DMPO-OH;  $a_N = 13.2$  G,  $a_H = 9.5$  G, 1.47 G, and 0.75 G for DMPO-SO<sub>4</sub>. Furthermore, the peak intensities of DMPO-OH and DMPO-SO<sub>4</sub> increased with increasing reaction time in the PS/V<sub>2</sub>O<sub>3</sub> system, and no significant EPR signal was observed in DMPO or PS solution alone. These results indicated that significant amounts of SO<sub>4</sub><sup>•-</sup> and •OH were generated during the initial stage of PS activation by a relatively small amount of V<sub>2</sub>O<sub>3</sub>, as compared to other PS activation processes described in previous studies [21,46].

##### 3.1.2. Free radical quenching studies

Free radical quenching studies were performed to further identify the contribution of SO<sub>4</sub><sup>•-</sup> and •OH to PCB28 degradation in V<sub>2</sub>O<sub>3</sub>/PS. Ethanol (EtOH) and *tert*-butyl alcohol (TBA) were used as selective radical scavengers, since their reaction rate constants with SO<sub>4</sub><sup>•-</sup> and •OH differ significantly. The second reaction rate constants of TBA are  $(4.0\text{--}9.4) \times 10^5 \text{ M}^{-1}\text{s}^{-1}$  and  $(3.8\text{--}7.6) \times 10^8 \text{ M}^{-1}\text{s}^{-1}$  with SO<sub>4</sub><sup>•-</sup> and •OH, respectively; while the second reaction rate constants of EtOH are  $(1.6\text{--}7.7) \times 10^7 \text{ M}^{-1}\text{s}^{-1}$  with SO<sub>4</sub><sup>•-</sup>, and  $(1.2\text{--}2.8) \times 10^9 \text{ M}^{-1}\text{s}^{-1}$  with •OH [47]. As shown in Fig. 2a, the degradation efficiency of PCB28 decreased significantly from 82% to 40% in V<sub>2</sub>O<sub>3</sub>/PS in the presence of 50 mM EtOH, which was ascribed to the fact that EtOH consumed SO<sub>4</sub><sup>•-</sup> and •OH, and thus inhibited PCB28 degradation. However, it is surprising that the degradation of PCB28 increased from 82% to 98% in V<sub>2</sub>O<sub>3</sub>/PS with addition of 50 mM TBA. The degradation of PCB28 followed pseudo-first-order kinetics (Fig. S3). The degradation rate constants ( $k_{obs}$ ) of PCB28 were 0.0072 and 0.0164 min<sup>-1</sup> in the absence and presence of TBA, respectively. The results indi-

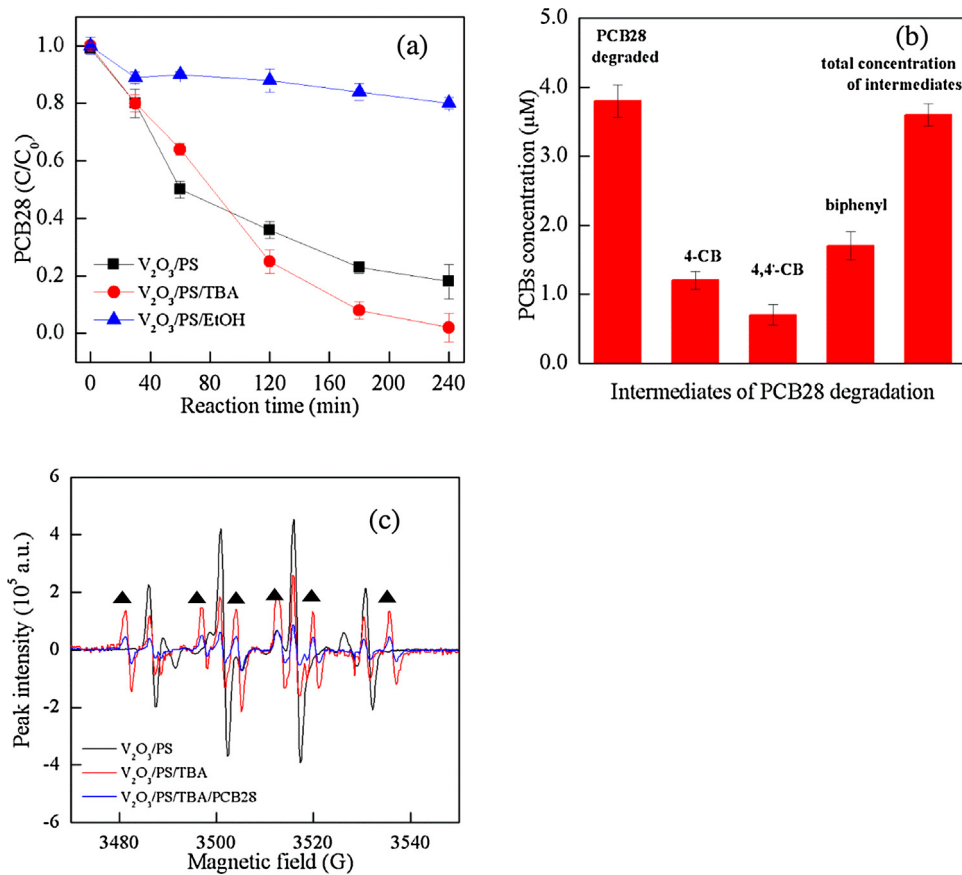
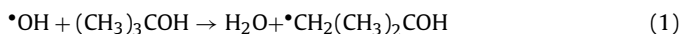


**Fig. 2.** Effects of scavengers on the degradation of PCB28 in  $V_2O_3/PS$ : (a) effects of TBA and EtOH on PCB28 degradation by  $V_2O_3/PS$ ; (b) products of PCB28 degradation in  $V_2O_3/PS$  in the presence of TBA; (c) EPR spectra of  $V_2O_3/PS$  in the presence of TBA and DMPO at 10 min. Reaction conditions:  $[PS]_0 = 2.0\text{ mM}$ ;  $V_2O_3$  loading:  $0.05\text{ g/L}$ ;  $[PCB28]_0 = 3.9\text{ }\mu\text{M}$ ;  $[EtOH]_0 = [TBA]_0 = 50\text{ mM}$ ;  $[DMPO]_0 = 100\text{ mM}$ ; pH 5.9 and  $25^\circ\text{C}$ . Black triangle: DMPO- $\text{CH}_2(\text{CH}_3)_2\text{OH}$ .

cated that TBA enhanced PCB28 degradation in  $V_2O_3/PS$ , which was inconsistent with previous reported experimental results that TBA usually acted as scavenger of  $\text{SO}_4^{\bullet-}$  and  $\bullet\text{OH}$ , and inhibited contaminant degradation [42].

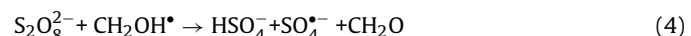
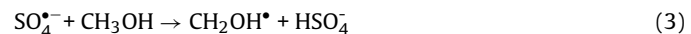
The possible reason was that  $\text{SO}_4^{\bullet-}$  and  $\bullet\text{OH}$  were converted to alcohol radicals ( $\bullet\text{CH}_2(\text{CH}_3)_2\text{COH}$ ) according to Eqs. (1) and (2), which were further involved in the degradation of PCB28 in  $V_2O_3/PS/TBA$ . It has been reported that alcohol radicals such as  $\bullet\text{CH}_2\text{OH}$ ,  $\bullet\text{CH}_2\text{CH}_2\text{OH}$  and  $\bullet\text{CH}_2(\text{CH}_3)_2\text{COH}$  have strong reducing ability with reduction potential of  $-1.39\sim -1.18\text{ V}$ , and thus are capable of reductively degrading contaminants [48,49].



Therefore, it was hypothesized that  $\bullet\text{CH}_2(\text{CH}_3)_2\text{COH}$  radical degraded PCB28 via reductive dechlorination process in  $V_2O_3/PS/TBA$ . To testify this hypothesis, the intermediates of PCB28 degradation were quantified in  $V_2O_3/PS/TBA$ . As shown in Fig. 2b, the dechlorination products such as 4-CB, 4,4'-CB and biphenyl were observed in the reaction system within 240 min, and their corresponding concentrations were  $1.2$ ,  $0.7$  and  $1.7\text{ }\mu\text{M}$ , respectively. The total concentration of these intermediates was  $3.6\text{ }\mu\text{M}$ , which accounted for  $92.3\%$  of PCB28 degraded ( $3.9\text{ }\mu\text{M}$ ) in  $V_2O_3/PS/TBA$ , indicating that reductive dechlorination was the dominant process for PCB28 degradation. These dechlorination products of PCB28 were not observed in  $V_2O_3/PS$  in the absence of TBA, and GC-MS analysis of the products will be discussed in the following section (Fig. S7).

Furthermore, EPR analysis showed that signals of DMPO-OH and DMPO- $\text{SO}_4^-$  were greatly suppressed in the presence of TBA, accompanied with formation of a new DMPO adducts with peak intensities of  $1:1:1:1:1$ , which was characteristic of DMPO- $\text{CH}_2(\text{CH}_3)_2\text{OH}$  according to previous studies (Fig. 2c) [45]. In the presence of PCB28 ( $3.9\text{ }\mu\text{M}$ ), the peak intensity of DMPO- $\text{CH}_2(\text{CH}_3)_2\text{OH}$  decreased markedly, and was only about  $1/3$  of that without PCB28, which suggested that alcohol radical was consumed during the dechlorination of PCB28 in  $V_2O_3/PS/TBA$ . These results indicated that alcohol radicals formed from the reactions of alcohol and  $\text{SO}_4^{\bullet-}$  or  $\bullet\text{OH}$  would participate in the dechlorination of PCB28. However, the dechlorination of PCB28 did not occur in the presence of EtOH in the  $V_2O_3/PS$  system.

It has been reported that the following reactions would occur during persulfate activation processes in the presence of methanol [50].



According to these reactions, it was found that alcohol radical was consumed with persulfate ions ( $\text{S}_2\text{O}_8^{2-}$ ) or self-recombination in the PS activation process. However, the consumption of one molecule alcohol radical (AR) would produce one molecule  $\text{SO}_4^{\bullet-}$ , which further reacts with alcohol to produce another molecule of AR. Furthermore, the second reaction rate constant of Eq. (3) was  $(1.6\text{--}7.7) \times 10^7\text{ M}^{-1}\text{s}^{-1}$  for EtOH, which was significantly higher than that of Eq. (4) (about  $10^4\text{ M}^{-1}\text{s}^{-1}$  for EtOH, as approximated by the second order rate constant of EtOH radical and  $\text{H}_2\text{O}_2$ ) [51]. The

concentration of alcohol was higher than that of  $S_2O_8^{2-}$ . Although self-recombination reaction (Eq. (5)) rate constants of alcohol radicals were about  $10^9 M^{-1} s^{-1}$  [52], this reaction was less more important than Reaction (3) and (4), since their concentrations ( $\sim 10^{-13} M$ ) were significant lower than that of reactants in Eq. (3) and (4). Consequently, the Eq. (3) was predominated, and sulfate radical was rapidly consumed in the free radical quenching studies and the reaction was terminated by forming aldehydes or ketones during the persulfate activation process. In our reaction system ( $V_2O_3/PS/TBA$  and  $V_2O_3/PS/TBA$ ), the alcohol was excessive with concentration of 50 mM, while PS concentration was only 2 mM. Moreover, the formation of  $SO_4^{•-}$  from PS activation with  $V_2O_3$  also consumed persulfate (Fig. 1b).

Therefore, PS concentration would play an important role in affecting the formation of AR in the quenching reaction systems, and its concentration was determined in the  $V_2O_3/PS/TBA$  and  $V_2O_3/PS/EtOH$  systems, respectively. As shown in Fig. S4, the decomposition of PS was markedly enhanced in the presence of TBA and EtOH. PS was almost completely disappeared in the presence of EtOH, while PS only 25% was consumed in the presence of TBA within 30 min. These results indicated that EtOH as an efficient quencher for both  $SO_4^{•-}$  and  $•OH$  radicals would result in rapid decomposition of PS in  $V_2O_3/PS/EtOH$ . However, slower reaction between TBA and  $SO_4^{•-}$ , which has second order rate constant about 100 times smaller than that of EtOH, resulted in continuous generation of TBA radicals during the prolonged reaction time. It has been observed that alcohol radicals produced by gamma irradiation are capable of reductive dechlorination of PCBs [53]. Similarly, TBA radical would play an important role in the degradation of PCB28 in the  $V_2O_3/PS$  system, which would be significantly affected by both the concentration and reactivity of the alcohol radical toward PCB28.

In-situ FTIR spectroscopy with the attenuated total reflection technique (ATR) was used to further testify the process of PCB28 dechlorination in the  $V_2O_3/PS/TBA$  system. Due to the detection limit of ATR-FTIR, higher concentration of PCB28 ( $\sim 1$  mg/g) was firstly loaded on the surface of  $V_2O_3$  particles to examine the degradation of PCB28 on the surface, and then PS solution was added to react with  $V_2O_3$  for PCB28 degradation. The simulated FTIR spectra of PCB28 and its major dechlorination products (BP, 4,4'-CB, 4-CB) were obtained by DFT calculations with MPWPW91 functional and 6-31+G\*\* basis set using Gaussian software package, and solvation effects were accounted by SMD model [54,55]. As shown in Figs. S5 and S6, the main peaks of PCB28 bands are at 1453.1, 1108.9 and 984  $cm^{-1}$  in aqueous solutions, which shifted to 1516.5, 1099.9 and 941.8  $cm^{-1}$  on the surface of  $V_2O_3$  particles. In the presence of PS and TBA, the main peaks of PCB28 (bands at 1516.5) decreased, but the initial rate of PCB28 degradation was significantly lower than that without TBA (Fig. S6). This is due to the fact that TBA inhibited PCB28 degradation at the beginning of the reaction (within 60 min as in Fig. 2b in the manuscript), and then PCB28 degradation was enhanced as reaction proceeded. Meanwhile, a growing peak was observed (647  $cm^{-1}$ ), which was the characteristic peak of biphenyl (BP) and less chlorinated biphenyls (4-CB and 4,4'-CB). The peak was not shown in reaction system without TBA (Fig. S6). Therefore, it was evidenced that dechlorinated products, such as BP, 4-CB and 4,4'-CB were formed on the  $V_2O_3$  surface in the presence of TBA. The ATR-FTIR results provide a further support for the dechlorination reaction of PCB28 in the  $V_2O_3/PS$  in the presence of TBA and surface site occupation by the formed metabolites.

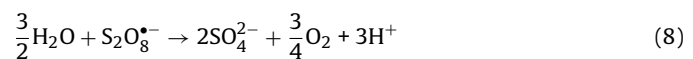
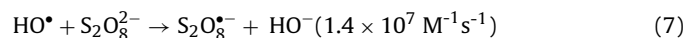
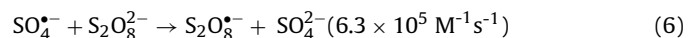
On the whole, free radical quenching studies was not effective in identifying the contribution of different free radicals ( $SO_4^{•-}$  and  $•OH$ ) for PCB28 degradation in the present study. However, according to the EPR results and previous studies, both  $SO_4^{•-}$  and  $•OH$  would contribute to PCB28 degradation. The distribution of free radicals in PS activation process is pH-dependent [41]. Although

the concentration of  $•OH$  under the present reaction pH (5.9) was only about 5% of  $SO_4^{•-}$  concentration in PS activation system, its reaction rate constant with PCB28 was about 1–2 orders of magnitude higher than that of  $SO_4^{•-}$  with PCB28, which resulted in appreciable contribution of  $•OH$  to PCB28 degradation [41,56].

### 3.1.3. Effects of PS concentration and $V_2O_3$ loading on PCB28 degradation

The Effect of  $V_2O_3$  loading on PCB28 degradation was studied. As shown in Fig. 3a (Fig. S7), PCB28 (3.9  $\mu$ M) was completely degraded by PS (2.0 mM) within 240 min in the presence of 0.1 or 0.2 g/L  $V_2O_3$  particles. While increasing  $V_2O_3$  loading from 0.2 to 1.0 g/L, the degradation efficiency of PCB28 decreased from 100% to 61%. The  $k_{obs}$  of PCB28 degradation increased rapidly from 0.4439 to 0.8876  $h^{-1}$  with increasing  $V_2O_3$  loading from 0.05 to 0.2 g/L; however, the  $k_{obs}$  decreased to 0.2279  $h^{-1}$  with a further increase in the  $V_2O_3$  loading to 1.0 g/L (Fig. 3b). Thus, the degradation of PCB28 depends on  $V_2O_3$  loading. The likely reason was that an increase in the amount of  $V_2O_3$  increased the activation of PS and degradation of PCB28. However, an excess of  $V_2O_3$  would also consume  $SO_4^{•-}$  and  $•OH$  available for PCB28 degradation. The decomposition of PS with different  $V_2O_3$  loadings was also examined. As shown in Fig. S7b, the decomposition of PS increased rapidly with increasing  $V_2O_3$  loadings, and can be well described with zero-order kinetics. The rate of PS decomposition ( $k_{obs}$ ) increased markedly from 0.0069 to 0.0309  $M \cdot min^{-1}$  as increased  $V_2O_3$  loading from 0.05 to 1.0 g/L (Fig. S7c). These results indicated that heterogeneous reaction was the dominant process for PS activation with  $V_2O_3$  to form free radicals.

Fig. 3c and d show the effects of PS concentration on PCB28 degradation. The  $k_{obs}$  of PCB28 degradation increased from 0.0094 to 0.0117  $min^{-1}$  with increasing PS concentration from 0.5 to 1.0 mM, and then decreased to 0.0078  $min^{-1}$  as PS concentration increased up to 10 mM within 240 min in  $V_2O_3/PS$  (Fig. S8 and Fig. 3d). This phenomenon was due to the fact that excessive PS ( $S_2O_8^{2-}$ ) would compete with PCB28 for the consumption of  $SO_4^{•-}$  and  $•OH$  according to the following reactions (Eqs. (6)–(8)) [57–59].



Consequently, excessive amount of PS inhibited PCB28 degradation. These results indicated that  $V_2O_3$  exhibited the excellent ability to activate PS for PCB28 degradation, even at relatively low PS concentration (0.5 mM).

### 3.1.4. Effects of pH on PCB28 degradation and vanadium leaching

The pH is an important factor affecting the distribution of free radical and the degradation of contaminants in PS activation process [60]. In the PCB28 degradation experiments described above, pH was not buffered, while decreased from 5.9 to 3.8 at the end of the reaction due to the decomposition of PS. Consequently, the acidic reaction solution led to dissolution of vanadium ions from  $V_2O_3$ , and 5.5 mg/L vanadium was detected in  $V_2O_3/PS$ . To reduce the dissolution of vanadium ions from  $V_2O_3$ , batch experiments were conducted at pH 7.4 and 8.4 with buffer solution (50 mM borate). As shown in Fig. 4a, 35% of PCB28 was degraded by PS (2.0 mM) activation with  $V_2O_3$  (0.05 g/L) at pH 7.4 within 240 min, while 27% of PCB28 was degraded with increasing pH to 8.4. Meanwhile, the PS concentration decreased from 2.0 to 1.7 and 1.8 mM for pH 7.4 and pH 8.4, respectively, while decreased to 0.4 mM at initial pH 5.9 without buffer (Fig. 4b). These results indicated that heterogeneous catalytic reactions occurred at both pH 7.4 and 8.4,

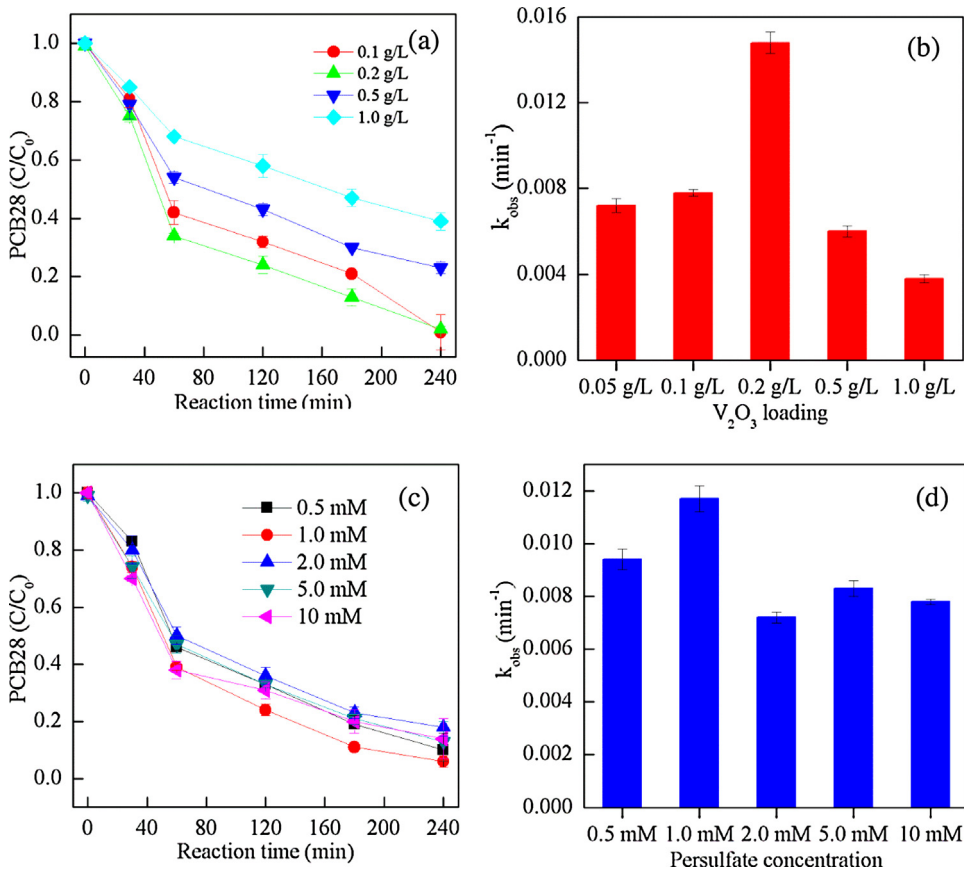


**Fig. 3.** Effects of  $V_2O_3$  loading and PS concentration on PCB28 degradation: (a) degradation kinetics of PCB28 as the function of  $V_2O_3$  loadings; (b) pseudo –first-order rate constants ( $k_{obs}$ ) of PCB28 degradation with different  $V_2O_3$  loadings; (c) effects of PS concentration on PCB28 degradation in  $V_2O_3$ /PS; (d)  $k_{obs}$  of PCB28 degradation with varies of PS concentration. Reaction conditions:  $[\text{PS}]_0 = 0.5 \sim 10 \text{ mM}$ ;  $V_2O_3$  loading:  $0.1 \sim 1.0 \text{ g/L}$ ;  $[\text{PCB28}]_0 = 3.9 \mu\text{M}$ ; pH 5.9 and  $25^\circ\text{C}$ .

whereas PS decomposed slowly on the surface of  $V_2O_3$  particles to produce  $\text{SO}_4^{2-}$  for PCB28 degradation.

Additionally, the degradation efficiency of PCB28 increased from 35% to 66% as  $V_2O_3$  loading increased from 0.05 to 0.2 g/L at pH 7.4, which indicated that increasing  $V_2O_3$  loading favored PS activation and PCB28 degradation (Fig. 4c). The concentration of vanadium dissolved from  $V_2O_3$  at pH 5.9 was 5.5, 9.3 and 14.3 mg/L for 0.05, 0.1 and 0.2 g/L  $V_2O_3$  loadings, respectively; while the dissolved vanadium concentration was 0.1, 0.2 and 0.25 mg/L, respectively, at pH 7.4 under the same reaction conditions. These results indicated that PS can be activated with  $V_2O_3$  for PCB28 degradation at neutral pH values.

### 3.2. Mechanism of PCB28 degradation and PS activation in $V_2O_3$ /PS system

#### 3.2.1. Proposed pathways for PCB28 degradation in $V_2O_3$ /PS

To elucidate the mechanisms of PCB28 degradation in  $V_2O_3$ /PS, GC-MS was applied to identify the intermediates of PCB28 degradation in  $V_2O_3$ /PS. As shown in Fig. S9, diethyl malonic acid (retention time: 4.4 min), 4-chlorobenzoic acid (4-CBA, 10.1 min), and 2,4-dichlorobenzoic acid (2,4-D, 12.12 min) were found to be the predominant intermediates of PCB28 degradation. To further examine the possible pathways of PCB28 degradation, the concentrations of 4-CBA, 2,4-D and  $\text{Cl}^-$  ion as function of reaction time were determined. As shown in Fig. 5a, both 4-CBA and 2,4-D concentrations reached maximum up to 0.77 and 0.48  $\mu\text{M}$ , respectively, when the reaction time reached 120 min, while decreased to 0.46 and 0.19  $\mu\text{M}$ , respectively, after 240 min. The results indicated that 4-CBA and 2,4-D markedly were accumulated at the begin-

ning of the reaction within 120 min, and then degraded as reaction proceeded from 120 to 240 min. Moreover, the  $\text{Cl}^-$  concentration increased markedly from 0 to 7.4  $\mu\text{M}$  within 240 min.

According to previous report about the proposed pathways of PCBs degradation by  $\text{SO}_4^{2-}$  and  $\cdot\text{OH}$  [42,61], and our GC-MS results, the likely pathways of PCB28 degradation in  $V_2O_3$ /PS are proposed in Scheme 1.  $\text{SO}_4^{2-}$  transfers an electron to the aromatic ring leading to the formation of a PCB-radical. Hydrolysis of PCB-radicals leads to the formation of chlorinated hydroxycyclohexadienyl radicals (CHRs). The attacks of  $\cdot\text{OH}$  on carbon (C) bonded with two aromatic rings also contributed to the formation CHRs similar to the pathway reported in the previous study [62]. CHRs further react with  $\text{O}_2$  giving rise to 4-CBA, 2,4-D and other chlorinated cleaved products. Then 4-CBA and 2,4-D were further degraded with  $\text{SO}_4^{2-}/\cdot\text{OH}$  to form diethyl malonic acid; diethyl malonic acid and chlorinated cleaved products were degraded to produce some other intermediates, which were finally mineralized to  $\text{CO}_2$  and  $\text{H}_2\text{O}$ . To support the proposed pathways of PCB28 degradation illustrated in Scheme 1, the mass balance of Cl concentration from PCB28 degraded ( $3[\text{PCB28 degraded}]$ ) and intermediates ( $[4\text{-CBA}] + 2[2,4\text{-D}] + [\text{Cl}^-]$ ) formed was calculated. Fig. 5b shows that the sum of Cl concentration obtained from the intermediates was only accounted for 34.6% of the total Cl concentration calculated from the complete mineralization of degraded PCB28 within 30 min, which indicated some chlorinated cleaved products were produced in these processes. As prolonging the reaction time to 240 min, the percentage of Cl gradually increased from 34.6% to 85.9%, which indicated the mineralization of these intermediates would occur in the  $V_2O_3$ /PS.

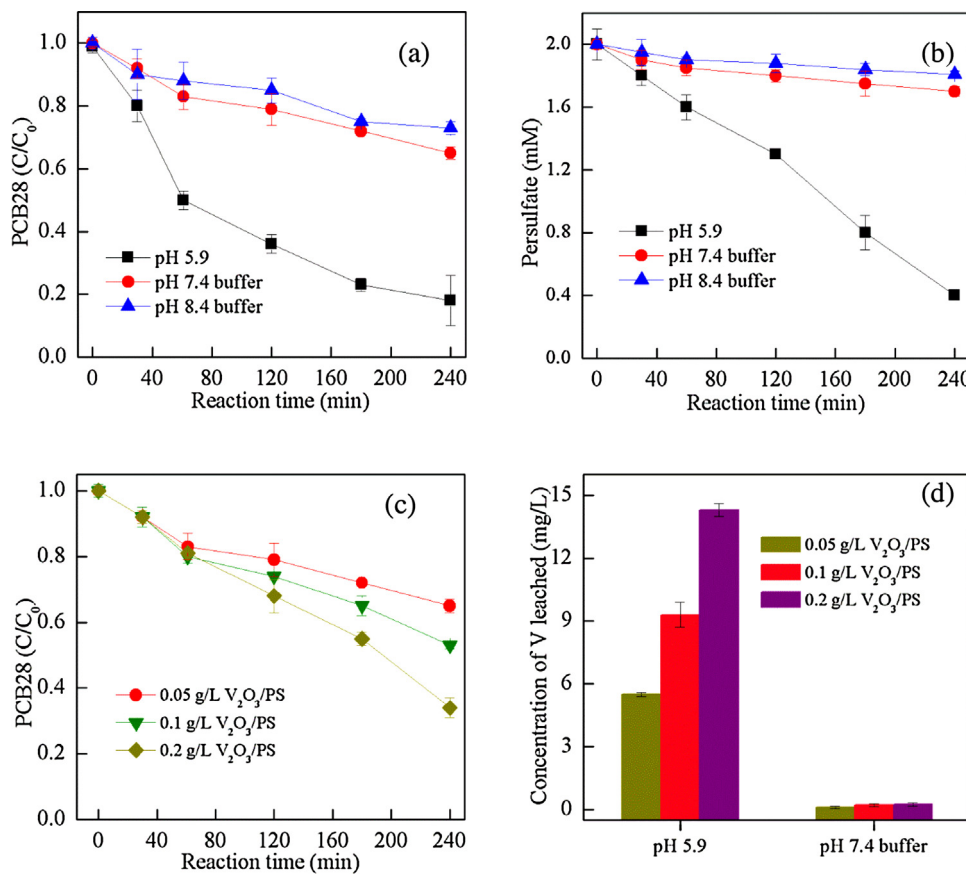


**Fig. 4.** Effects of pH on PCB28 degradation in  $V_2O_3/PS$ : degradation kinetics of PCB28 (a) and decomposition of PS (b) in  $V_2O_3/PS$  at pH 7.4 and 8.4 (50 mM borate buffer); (c) effects of  $V_2O_3$  loadings on PCB28 degradation in  $V_2O_3/PS$  at pH 7.4; (d) concentration of dissolved V from  $V_2O_3$  in  $V_2O_3/PS$  at pH 5.9 and 7.4. Reaction conditions: Reaction conditions:  $[PS]_0 = 2.0\text{ mM}$ ;  $V_2O_3$  loading:  $0.05 \sim 0.2\text{ g/L}$ ;  $[PCB28]_0 = 3.9\text{ }\mu\text{M}$ ; pH 7.4, 8.4 (50 mM borate buffer) and  $25^\circ\text{C}$ .

Persulfate (PS) heterogeneous activation by minerals for contaminant degradation is a multi-step and complicated process, due to the coexistence of PS and contaminants on the surface of minerals. The free radicals are firstly formed on the surface of minerals and thereby degrade the contaminants adsorbed on the surface of particles. However, the free radicals can also diffuse to aqueous solution and contribute to contaminant degradation. Therefore, both the heterogeneous and homogeneous reactions account for contaminants degradation in PS heterogeneous activation process as evidenced by the studies of PS with other minerals, including goethite ( $\alpha\text{-FeOOH}$ ), amorphous ferrihydrite ( $Fe(OH)_3$ ) and pyrolusite ( $\beta\text{-MnO}_2$ ) [22]. We conducted additional kinetic experiments and tried to elucidate the kinetics of PCBs degradation and PS activation in the  $V_2O_3/PS/PCBs$  system.

ATR-FTIR was used to verify the degradation of PCB28 on the surface of  $V_2O_3$  in the presence of PS. The FTIR spectra of in-situ reactions were firstly collected to examine the possible transformation of PCB28 on the surface of  $V_2O_3$ . And the spectra were compared to the simulated FTIR spectra of PCB28 and its major metabolites (2,4-D, 4-CBA), which were obtained by DFT calculations with MPWPW91 functionals and 6-31+G\*\* basis set using Gaussian 09 software package, and solvation effects were accounted by SMD model [54,55]. The vibrational frequencies were calculated on the optimized structures and were adjusted by a scaling factor of 0.932545. As shown in Fig. S6, by adding PS to the in-situ suspension, the main peaks of PCB28 (bands at  $1516.5\text{ cm}^{-1}$ ) decreased rapidly, accompanied with the formation of new peaks with increasing intensities (bands d and e at  $838$  and  $1011\text{ cm}^{-1}$ , which were attributed to stretching and bending modes of the produced  $SO_4^{2-}$ ), which was ascribed to the rapidly decomposition of

PS activation with  $V_2O_3$ . These results indicated that PCB28 can be efficiently degraded on the surface of  $V_2O_3$  in the presence of PS. The signal of metabolites of PCB28 such as 4-CBA and 2,4-D were not observed due to the relatively low concentrations on the surface of  $V_2O_3$  and the rapid further conversion of the metabolites during the reaction process.

EPR technique was used to testify the possibility that free radical diffuse from the surface of  $V_2O_3$  particles to bulk solution. As shown in Fig. S10, the reaction was conducted in a syringe containing PS (2.0 mM) and  $V_2O_3$  particles (0.05 g/L), then the suspension was filtered by the 0.22  $\mu\text{m}$  membrane filter into a 2-ml bottle (containing 100 mM DMPO) with a reaction time of 5 min (to ensure minimum amount of V ions was dissolved during the time period). The filtrate was quickly mixed with DMPO and subject to direct EPR analysis. The signals of DMPO- $SO_4$  and DMPO-OH were observed in the filtrates. Compared to the insignificant signals in PS/DMPO in the absence of  $V_2O_3$ , it was indicated that the sulfate radical and hydroxyl radical formed on the surface of  $V_2O_3$  particles can diffuse into to the bulk solution and both heterogeneous and homogeneous reactions account for PCB28 degradation.

Furthermore, additional experiments were conducted to justify the kinetics of PCB28 degradation and the effects of PCB28 concentrations on  $k_{obs}$  of their degradation were studied. As shown in Fig. S11, the degradation of PCB28 with different initial PCB28 concentrations seemed to follow the pseudo-first-order equation well for the whole time course ( $R^2 > 0.95$ ). However, slight deviation from first-order kinetics was observed, as the initial reaction rates of PCB28 degradation within 60 min were all around  $0.04\text{ }\mu\text{M min}^{-1}$ , which was close to a constant and independent to the initial concentrations of PCB28 (2.0, 3.9 and  $7.8\text{ }\mu\text{M}$ , respectively), indicating

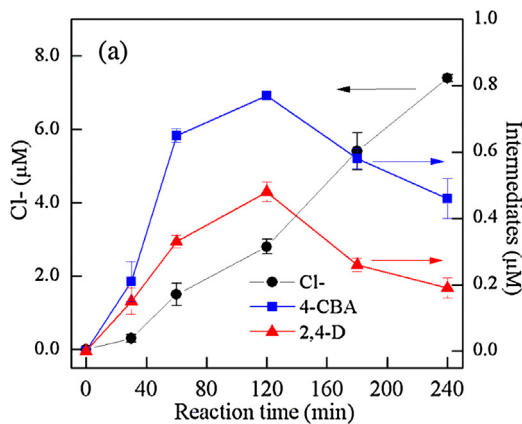
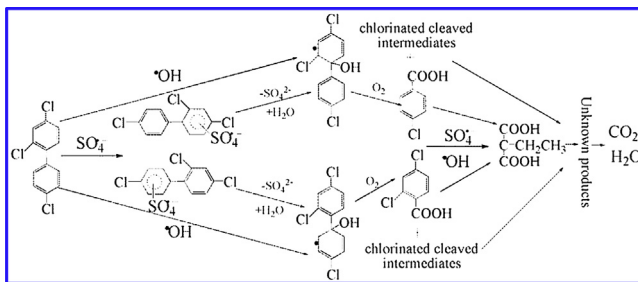
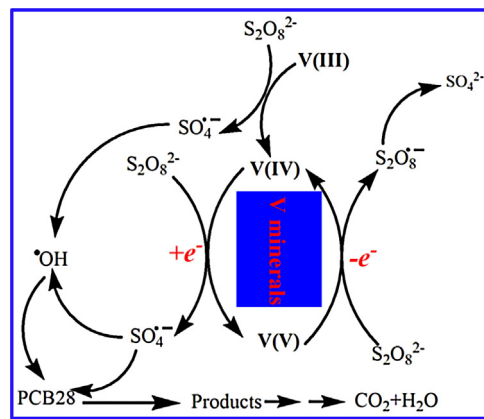


**Fig. 5.** Intermediates of PCB28 degradation in  $V_2O_3/PS$  system: (a) concentrations of 4-CBA, 2,4-D and chloride ion ( $Cl^-$ ) changed as the functions of the reaction time in  $V_2O_3/PS$ ; (b) mass balance of chloride ions between total (calculated from  $3[PCB28$  degraded]) and detected  $Cl^-$  (sum of detected  $Cl^-$ : [4-CBA] + 2[2,4-D] + [Cl-]). Reaction conditions:  $[PS]_0 = 2.0\text{ mM}$ ;  $V_2O_3$  loading:  $0.05\text{ g/L}$ ;  $[PCB28]_0 = 3.9\text{ }\mu\text{M}$ ; pH 5.9 and  $25^\circ\text{C}$ .



**Scheme 1.** Proposed pathway for PCB28 degradation in  $V_2O_3/PS$  system.

possible saturation of the surface reactive sites by reactant at high concentration. Similar to the previous study [63], a combined zero- and first-order kinetic model can be used to describe the PCB28 degradation process. At initial stage with higher PCB concentration, the degradation kinetics becomes zero-order due to the relatively limited surface area (the reactive sites) of micrometer-sized  $V_2O_3$  particles that could be saturated by PCB molecules, whereas for lower PCB concentration the kinetics is first-order indicating a transport-limited kinetics. It was, therefore, suggested that the observed pseudo-first-order degradation of PCB28 during the whole time course in PS activation with  $V_2O_3$  was a result of heterogeneous chemical reactions with first-order kinetics of transport (e.g., sorption, desorption, and reaction of the sorbed compound) included.



**Scheme 2.** Proposed pathways for persulfate activation with different vanadium species for sulfate radical generation.

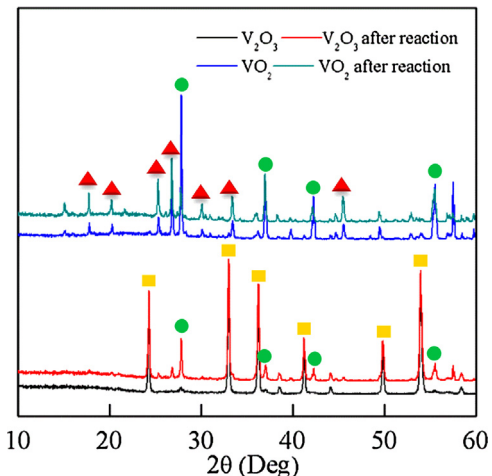
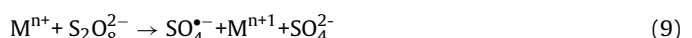


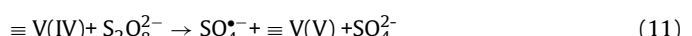
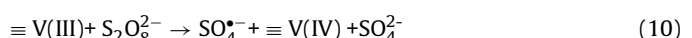
**Fig. 6.** XRD analysis of  $V_2O_3$  and  $VO_2$  particles before and after reaction during the activation of PS for PCB28 degradation. Reaction conditions:  $[PS]_0 = 2.0\text{ mM}$ ;  $V_2O_3/VO_2$  loadings:  $0.05\text{ g/L}$ ;  $[PCB28]_0 = 3.9\text{ }\mu\text{M}$ ; pH 5.9 and  $25^\circ\text{C}$ ; reaction time is 4 h and 24 h for  $V_2O_3/PS$  and  $VO_2/PS$ , respectively.  $V_2O_3$ : yellow diamonds;  $VO_2$ : green circles;  $VO_{13}$ : red triangle. (For interpretation of the references to colour in this figure legend, the reader is referred to the web version of this article.)

### 3.2.2. Proposed pathways for PS activation to produce sulfate radical

Contaminants have been effectively degraded by the activation of PS with transition metals [64]. The proposed mechanisms of PS activation by transition metals are as follows: low-valent metals transfer electrons to PS, forming  $SO_4^{•-}$  according to the following reaction;  $SO_4^{•-}$  react with  $H_2O$  or  $OH^-$  ions, generating  $•OH$ .



According to the previous studies and experimental results obtained in this study, **Scheme 2** shows the proposed pathways for PS activation by  $V_2O_3$ .  $V(III)$  in  $V_2O_3$  (denoted as  $\equiv V(III)$ ) transfers an electron to PS yielding  $SO_4^{•-}$  and  $\equiv V(IV)$ ;  $\equiv V(IV)$  further activates PS to produce  $SO_4^{•-}$  according to the following reactions.



To further verify the Reactions (10) and (11) occurred, XRD was employed to characterize the  $V_2O_3$  particles before and after reaction. As shown in **Fig. 6**, only  $V_2O_3$  phase was observed before reaction with diffraction peaks at  $2\theta$  of  $24.3$ ,  $33$ ,  $36.3$ ,  $41.2$ ,  $44.1$ ,  $49.8$  and  $53.9^\circ$  (PDF#65-9474), but some new phase appeared

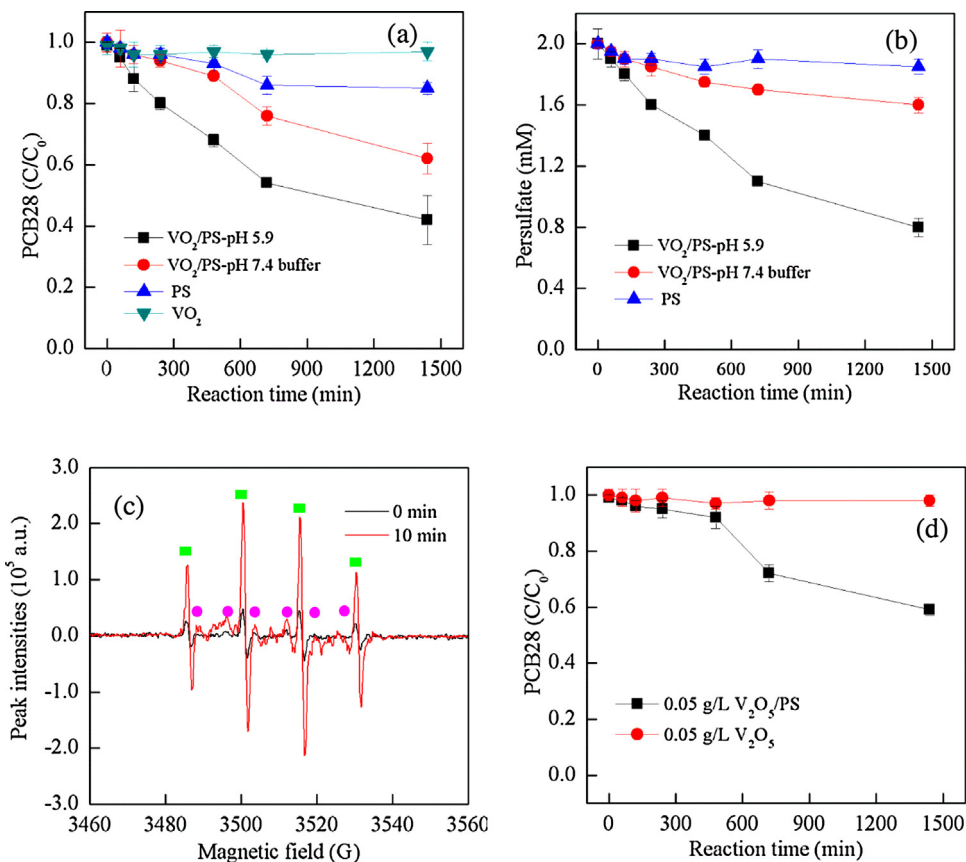


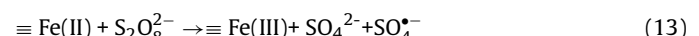
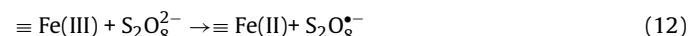
**Fig. 7.** Activation of PS with  $\text{VO}_2$  and  $\text{V}_2\text{O}_5$  for PCB28 degradation: (a) kinetics of PCB28 degradation and (b) PS decomposition in  $\text{VO}_2/\text{PS}$  at pH 5.9 and 7.4; (c) EPR spectra of  $\text{VO}_2/\text{PS}$  with DMPO as spin-trapping agent at pH 5.9; (d) kinetics of PCB28 degradation in  $\text{V}_2\text{O}_5/\text{PS}$  at pH 5.9. Reaction conditions:  $[\text{PS}]_0 = 2.0 \text{ mM}$ ;  $\text{VO}_2/\text{V}_2\text{O}_5$  loading:  $0.05 \text{ g/L}$ ;  $[\text{PCB28}]_0 = 3.9 \mu\text{M}$ ;  $[\text{DMPO}]_0 = 100 \text{ mM}$ ; pH 5.9 (without buffer), 7.4 (50 mM borate buffer) and  $25^\circ\text{C}$ . Green square: DMPO-OH; pink circle: DMPO-SO<sub>4</sub>. (For interpretation of the references to colour in this figure legend, the reader is referred to the web version of this article.)

after reaction with diffraction peaks at  $2\theta$  of 27.9, 37.1, 42.3 and 55.6°, which are characteristic peaks of crystalline  $\text{VO}_2$  according to PDF#37-2362. These results clearly indicated that  $\equiv\text{V(III)}$  in  $\text{V}_2\text{O}_3$  was oxidized to  $\equiv\text{V(IV)}$  during the activation of PS.

To examine the possibility that  $\equiv\text{V(IV)}$  activated PS via reaction (8), commercial  $\text{VO}_2$  was used to activate PS for PCB28 degradation. As shown in Fig. 7a, 58% of PCB28 was degraded by PS in the presence of  $0.05 \text{ g/L}$   $\text{VO}_2$  within 24 h (1440 min) at pH 5.9; 38% of PCB28 was degraded when the pH increased to 7.4 (buffer) under the same reaction conditions. In contrast, approximately 10–15% of PCB28 was degraded in the presence of PS alone within 24 h. The PS concentration decreased from 2.0 to 0.8 and 1.6 mM for pH 5.9 and 7.4, respectively. These results indicated that  $\text{VO}_2$  also can activate PS for PCB28 degradation. Similar degradation intermediates such as diethyl malonic acid, 4-CBA and 2,4-D were observed in the  $\text{VO}_2/\text{PS}$  system, which were similar to those formed in the  $\text{V}_2\text{O}_3/\text{PS}$  system, indicating that a similar degradation process occurred in the V/PS systems (Fig. S12). Fig. 7c shows the EPR spectra of  $\text{VO}_2/\text{PS}$  suspension at 0 and 10 min at pH 5.9. The DMPO-SO<sub>4</sub> and DMPO-OH signals were also detected, which indicated the formation of SO<sub>4</sub><sup>2-</sup> and •OH in PS activation with  $\text{VO}_2$ . These results give direct evidence to support Reaction (8). XRD was employed to further characterize  $\text{VO}_2$  before and after reaction. Fig. 6 shows that the commercial  $\text{VO}_2$  contains about 24% of  $\text{V}_6\text{O}_{13}$  (peaks at  $2\theta$ : 15.2, 17.8, 25.4, 26.5, 30.2, 33.6 and 45.6°, PDF#72-1278), which was ascribed to partial oxidation of  $\text{VO}_2$ .  $\text{V}_6\text{O}_{13}$  is a mixed valent oxide of  $\text{VO}_2$  and  $\text{V}_2\text{O}_5$ , and contains both V(IV) and V(V) species. After reaction, new peaks were not observed, but the proportion of  $\text{V}_6\text{O}_{13}$  increased from 24% to 62%, while  $\text{VO}_2$  decreased from 74% to 38%.

These results indicated that  $\equiv\text{V(IV)}$  was oxidized to  $\equiv\text{V(V)}$  during the activation of PS by  $\text{VO}_2$ , which resulted in the formation of more  $\text{V}_6\text{O}_{13}$ .

The regeneration of  $\equiv\text{V(IV)}$  from the reduction of  $\equiv\text{V(V)}$  would be an important factor controlling the catalytic ability of  $\text{V}_2\text{O}_5$ . It has been reported that  $\equiv\text{Fe(II)}$  would be produced from the reduction of  $\equiv\text{Fe(III)}$  by persulfate ions (S<sub>2</sub>O<sub>8</sub><sup>2-</sup>) during the activation of PS with Fe(III)-containing minerals according to the following reactions [65]:



Therefore, similar to the mechanism for the activation of PS by Fe(III)-containing minerals, a pathway of  $\equiv\text{V(IV)}$  regeneration in  $\text{V}_2\text{O}_5/\text{PS}$  can be proposed as follows:



The one-electron reduction of  $\equiv\text{V(V)}$  affords  $\equiv\text{V(IV)}$  on the surface of  $\text{V}_2\text{O}_5$  particles.  $\equiv\text{V(IV)}$  further reacts with PS, generating SO<sub>4</sub><sup>2-</sup> for PCB28 degradation (reaction (11)). Activation of PS by  $\text{V}_2\text{O}_5$  for PCB28 degradation was used to verify this process. As shown in Fig. 7d, 41% of PCB28 (3.9  $\mu\text{M}$ ) was degraded within 24 h (1440 min) with PS activation with  $0.05 \text{ g/L}$   $\text{V}_2\text{O}_5$  at pH 5.9, while <10% of PCB28 disappeared under the same reaction conditions. Meanwhile, it was observed that only 8% of PCB28 was degraded at the beginning of reaction within 480 min, and then PCB28 was rapidly decayed after 480 min. The likely reason was that the amount of formed  $\equiv\text{V(IV)}$  sites from the reduction of  $\equiv\text{V(IV)}$  by S<sub>2</sub>O<sub>8</sub><sup>2-</sup> was not enough to induce PS activation and PCB28 degra-

dation at the beginning of the reaction. As reaction time proceeded, the amount of  $\equiv$ V(IV) increased, which efficiently activated PS for PCB28 degradation. Furthermore, V ions dissolved from vanadium oxides would partially contribute to PS activation for PCB28 degradation, particularly in the non-buffered reaction solutions.

To identify the contribution of V ions to PS activation for PCB28 degradation, the activation of PS with V(IV) ion was investigated. V(III) ion was unstable in aqueous solution and would be oxidized to V(IV) or V(V) in the presence of PS. Moreover, it was difficult to find a commercial compound of V(III) ion. Therefore, V(IV) ion ( $\text{VOSO}_4 \cdot \text{xH}_2\text{O}$ ) was selected to evaluate the role of V ions in PS activation. As shown in Fig. S13, there were no significant difference of PCB28 degradation as the function of V(IV) ion concentrations within 240 min, and about 16% of PCB28 was degraded in this process, whereas 82% of PCB28 degraded in the  $\text{V}_2\text{O}_3/\text{PS}$  system. The results indicated that V ions activation contributed to about 19.5% (16/82\*100) for PCB28 degradation in the PS/ $\text{V}_2\text{O}_3$  in the present study.

#### 4. Conclusions

Vanadium (V) is a redox-sensitive metal widely distributed in natural environment, particularly in soil, which would affect the remediation efficiency of contaminants by persulfate (PS)-based *in-situ* chemical oxidation. In the present study, the activation of persulfate with V species for the degradation of contaminants was reported for the first time. It was found that  $\text{V}_2\text{O}_3$  exhibited high catalytic activity toward PS decomposition for PCB28 degradation.  $\text{VO}_2$  and  $\text{V}_2\text{O}_5$  also can activate PS to degrade PCB28, although the efficiency of PCB28 degradation was significantly lower than that in the  $\text{V}_2\text{O}_3/\text{PS}$  system. Importantly, the PCB28 was degraded efficiently in  $\text{V}_2\text{O}_3/\text{PS}$  even under near neutral pH (7.4) and environmentally relevant vanadium loadings. For example, PS can be activated with 0.05 g/L  $\text{V}_2\text{O}_3$  (17 mg/L V),  $\text{VO}_2$  (30.7 mg/L V) and  $\text{V}_2\text{O}_5$  (14 mg/L V) for the degradation of PCB28 and formation of  $\text{SO}_4^{2-}$  in the V/PS system, whereas the vanadium loadings were significantly lower than the vanadium content in soil (90 mg/kg in the soil around the world) [27].

The mechanisms of PS activation and PCB28 degradation were proposed. It was found that diethyl malonic acid, 3-chlorobenzoic acid, and 2,4-dichlorobenzoic acid were the main intermediates of PCB28 degradation in  $\text{V}_2\text{O}_3/\text{PS}$ . The pathways of PCB28 degradation were proposed based on results of GC-MS analysis and the concentration of profiles of intermediates and chloride ion as function of reaction time. The V(III) in  $\text{V}_2\text{O}_3$  activated PS to form  $\text{SO}_4^{2-}$  and V(IV) ( $\text{VO}_2$ ) via electron transfer processes, and the formed V(IV) further transfer an electron to PS to generate  $\text{SO}_4^{2-}$  and V(V) ( $\text{V}_6\text{O}_{13}$ ). The V(IV) was regenerated from the reduction of V(V) by persulfate ions ( $\text{S}_2\text{O}_8^{2-}$ ). All these processes were supported with XRD analysis, and the fact that  $\text{VO}_2$  and  $\text{V}_2\text{O}_5$  can also activate PS for PCB28 degradation. EPR technique using DMPO as spin-trapping agent confirmed the formation of sulfate radical anions ( $\text{SO}_4^{2-}$ ) and hydroxyl radicals ( $\cdot\text{OH}$ ) in PS activation with vanadium species.

The findings of this study would help to better understand the interactions between naturally occurring vanadium minerals and PS, and provide a potential strategy for the degradation of contaminants in soils based on PS activation. Because vanadium species are present in soil environments in considerable concentrations, PS may be activated by vanadium species naturally for contaminants degradation without addition of other activators. From the view of waste water purification, the results of this study would also provide the possibility to develop vanadium-based naturally occurring minerals for the purification of waste water. Since these materials such as natural vanadium–titanium magnetite and vanadium doping magnetite nanoparticles has been successfully applied

to the decolorization of Acid Orange II and methylene blue based Fenton-like reactions in aqueous solutions [66,67].

#### Acknowledgments

This work was supported by the grants from the National Key Basic Research Program of China (2013CB934303), the National Natural Science Foundation of China (41401252, 41301535, 21307141), the Natural Science Foundation of Jiangsu Province of China (BK20141047, BK20131042), the 135 Program of Institute of Soil Science (ISSASIP1660), and Youth Innovation Promotion Association of CAS (2014270).

#### Appendix A. Supplementary data

Supplementary data associated with this article can be found, in the online version, at <http://dx.doi.org/10.1016/j.apcatb.2016.09.006>.

#### References

- [1] M.A. Dahman, K.H. Huang, G.E. Hoag, Water Air Soil Pollut. 6 (2006) 127–141.
- [2] R.L. Siegrist, M. Crimi, T.J. Simpkin, In *Situ Chemical Oxidation: Technology, Description and Status*. In *Situ Chemical Oxidation for Groundwater Remediation*, Springer Media, LLC, New York City, 2011 (Chapter 1.).
- [3] F.J. Krembs, R.L. Siegrist, M.L. Crimi, R.F. Furrer, B.G. Petri, Ground Water Monit. Rem. 30 (2010) 42–53.
- [4] A. Tsitonaki, B. Petri, M. Crimi, H. Mosbaek, R.L. Siegrist, P.L. Bjerg, Crit. Rev. Environ. Sci. Technol. 40 (2010) 55–91.
- [5] R.H. Waldemer, P.G. Tratnyek, R.L. Johnson, J.T. Nurmi, Environ. Sci. Technol. 41 (2007) 1010–1015.
- [6] Y.H. Guan, J. Ma, X.C. Li, J.Y. Fang, L.W. Chen, Environ. Sci. Technol. 45 (2011) 9308–9314.
- [7] J.M. Monteagudo, A. Durán, R. González, A.J. Expósito, Appl. Catal. B: Environ. 176–177 (2015) 120–129.
- [8] A. Rastogi, S.R. Al-Abed, D.D. Dionysiou, Appl. Catal. B: Environ. 85 (2009) 171–179.
- [9] O.S. Furman, A.L. Teel, R.J. Watts, Environ. Sci. Technol. 44 (2010) 6423–6428.
- [10] Y. Gao, Z. Zhang, S. Li, J. Liu, L. Yao, Y. Li, H. Zhang, Appl. Catal. B: Environ. 185 (2016) 22–30.
- [11] Y. Lei, C. Chen, Y. Tu, Y. Huang, H. Zhang, Environ. Sci. Technol. 49 (2015) 6838–6845.
- [12] B.A. Cavanagh, P.C. Johnson, E.J. Daniels, Environ. Sci. Technol. 48 (2014) 14582–14589.
- [13] N.B. Sutton, M. Kalisz, J. Krupanek, J. Marek, T. Grotenhuis, H. Smidt, J. Weert, H.M. Rijnaarts, P. Gaans, T. Keijzer, Environ. Sci. Technol. 48 (2014) 2352–2360.
- [14] C.K.O. da Silva-Rackov, W.A. Lawal, P.A. Nfodzo, M.M.G.R. Vianna, C.A.O. do Nascimento, H. Choi, Degradation of PFOA by hydrogen peroxide and persulfate activated by iron-modified diatomite, Appl. Catal. B 192 (2016) 253–259.
- [15] X.G. Duan, C. Su, L. Zhou, H.Q. Sun, A. Suvorova, T. Odedairo, Z.H. Zhu, Z.P. Shao, S.B. Wang, Surface controlled generation of reactive radicals from persulfate by carbocatalysis on nanodiamonds, Appl. Catal. B 194 (2016) 7–15.
- [16] K.S. Sri, N.R. Thomson, J.F. Barker, Environ. Sci. Technol. 44 (2010) 3098–3104.
- [17] M. Ahmad, A.L. Teel, R.J. Watts, Environ. Sci. Technol. 47 (2013) 5864–5871.
- [18] G.D. Fang, J. Gao, D.D. Dionysiou, S.R. Al-Abed, D.M. Zhou, Environ. Sci. Technol. 47 (2013) 4605–4611.
- [19] M. Ahmad, A.L. Teel, R.J. Watts, J. Contam. Hydrol. 115 (2010) 34–45.
- [20] A.L. Teel, M. Ahmad, R.J. Watts, J. Hazard. Mater. 196 (2011) 153–159.
- [21] G.D. Fang, D.D. Dionysiou, S.R. Al-Abed, D.M. Zhou, Appl. Catal. B: Environ. 129 (2013) 325–332.
- [22] H.Z. Liu, T.A. Bruton, F.M. Doyle, D.L. Sedlak, Environ. Sci. Technol. 48 (2014) 10330–10336.
- [23] E. Saputra, S. Muhammad, H.Q. Sun, H.M. Ang, M.O. Wang, S.B. Tade, Environ. Sci. Technol. 47 (2013) 5882–5887.
- [24] A. Boularbah, J.L. Morel, G. Bitton, M. Mench, J. Soil Contam. 5 (1996) 395–404.
- [25] J. Yang, Y. Tang, K. Yang, A.A. Rouff, E.J. Elzinga, J. Huang, J. Hazard. Mater. 264 (2014) 498–504.
- [26] C. Reimann, P. de Caritat, *Chemical Elements in the Environment*, Springer, Heidelberg, 1998.
- [27] R. Edwards, N.W. Lepp, K.C. Jones, Other less abundant elements of potential significance, in: B.J. Alloway (Ed.), *Heavy Metals in Soils*, 2nd edn., Blackie Academic and Professional, Chapman and Hall, London, 1995, pp. 307–352.
- [28] Y. Teng, J. Yang, Z. Sun, J. Wang, R. Zuo, J. Zheng, Environ. Monit. Assess. 176 (2011) 605–620.
- [29] M. Imtiaz, M.S. Rizwan, S.L. Xiong, H.L. Li, M. Ashraf, S.M. Shahzad, M. Shahzad, M. Rizwan, S.X. Tu, Environ. Int. 80 (2015) 79–88.

[30] D. Rehder, Transport, accumulation, and physiological effects of vanadium, in: Irena Sheremeti I, A. Varma (Eds.), *Detoxification of Heavy Metals*, 1st edn., Springer, New York, 2011.

[31] B.K. Hope, An assessment of the global impact of anthropogenic vanadium, *Biogeochemistry* 37 (1997) 1–13.

[32] M. Jensen-Fontaine, W.P. Norwood, M. Brown, D. George Dixon, X. Chris Le, *Environ. Sci. Technol.* 48 (2014) 731–738.

[33] I.E. Wachs, *Dalton Trans.* 42 (2013) 11762–11769.

[34] F. Buonomo, D. Sanfilippo, F. Trifiro, G. Ertl, H. Knözinger, J. Weitkamp, *Handbook of Heterogeneous Catalysis*, 5, Wiley-VCH, Weinheim, 1997, pp. 2140–2151.

[35] F. Trifiro, B. Grzybowska, *Appl. Catal. A* 157 (1997) 195–221.

[36] H.F. Rase, *Handbook of Commercial Catalysis*, CRC, New York, 2000.

[37] M. Nobbenhuis, A. Baiker, P. Barnickel, A. Wokaun, *Appl. Catal.* 85 (1992) 157–172.

[38] G. Bond, S. Tahir, *Appl. Catal.* 71 (1991) 1–31.

[39] C.A. Carrero, R. Schloegl, I.E. Wachs, R. Schomaeker, *ACS Catal.* 4 (2014) 3357–3380.

[40] D. Nitsche, C. Hess, Normal mode analysis of silica-supported vanadium oxide catalysts: comparison of theory with experiment, *Catal. Commun.* 52 (2014) 40–44.

[41] G.D. Fang, D.D. Dionysiou, Y. Wang, S.R. Al-Abed, D.M. Zhou, *J. Hazard. Mater.* 227–228 (2012) 394–401.

[42] G.D. Fang, D.D. Dionysiou, D.M. Zhou, Y. Wang, X.D. Zhu, J.X. Fan, L. Cang, Y.J. Wang, *Chemosphere* 90 (2013) 1573–1580.

[43] C. Liang, C.F. Huang, N. Mohanty, R.M. Kurakalva, *Chemosphere* 73 (2008) 1540–1543.

[44] C. Liang, C.J. Bruell, M.C. Marley, K.L. Sperry, *Soil Sediment Contam.* 12 (2003) 207–228.

[45] G.D. Fang, C. Liu, J. Gao, D.D. Dionysiou, D.M. Zhou, *Environ. Sci. Technol.* 49 (2015) 5645–5653.

[46] W. Oh, Z. Dong, T. Lim, *Appl. Catal. B* 194 (2016) 169–201.

[47] C. Liang, H.W. Su, *Ind. Eng. Chem. Res.* 48 (2009) 5558–5562.

[48] H.A. Schwarz, R.W. Dodson, *J. Phys. Chem.* 93 (1989) 409–414.

[49] G.R. Peyton, E. Girin, M.H. Lefaivre, *Environ. Sci. Technol.* 29 (1995) 1710–1712.

[50] P.D. Bartlett, J.D. Cotman, *J. Am. Chem. Soc.* 71 (1949) 1419–1422.

[51] E. Popov, M. Mametkuliyev, D. Santoro, L. Liberti, J. Eloranta, *Environ. Sci. Technol.* 44 (2010) 7827–7832.

[52] S.P. Mezyk, K.P. Madden, *J. Phys. Chem. A* 103 (1999) 235–242.

[53] T. Sawai, T. Shimokawa, Y. Shinozaki, *Bull. Chem. Soc. Jpn.* 47 (1974) 1889–1893.

[54] M.J. Frisch, G.W. Trucks, H.B. Schlegel, G.E.M.A. Scuseria, J.R. Robb, G. Cheeseman, V. Scalmani, B. Barone, G.A. Mennucci, H. Petersson, M. Nakatsuji, X. Caricato, H.P. Li, A.F. Hratchian, J. Izmaylov, G. Bloino, J.L. Zheng, M. Sonnenberg, M. Hada, K. Toyota Ehara, R. Fukuda, J. Hasegawa, M. Ishida, T. Nakajima, Y. Honda, O. Kitao, T. Vreven, J. A. Jr. Montgomery, J.E. Peralta, F. Ogliaro, M. Bearpark, J.J. Heyd, E. Brothers, K.N. Kudin, V.N.R. Staroverov, J. Kobayashi, K. Normand, A. Raghavachari, J.C. Rendell, S.S. Burant, J. Iyengar, M. Tomasi, N. Cossi, J.M. Rega, M. Millam, J.E. Klene, J.B. Knox, V. Cross, C. Bakken, J. Adamo, R. Jaramillo, R.E. Gomperts, O. Stratmann, A.J. Yazyev, R. Austin, C. Cammi, J.W. Pomelli, R.L. Ochterski, K. Martin, V.G. Morokuma, G.A. Zakrzewski, P. Voth, J.J. Salvador, S. Dannenberg, A.D. Dapprich, O. Daniels, J.B. Farkas, J.V. Foresman, J. Ortiz, D.J. Cioslowski, Gaussian 09, Revision B.01, Gaussian, Inc., Wallingford, CT, 2009.

[55] A.V. Marenich, C.J. Cramer, D.G. Truhlar, *J. Phys. Chem. B* 113 (2009) 6378–6396.

[56] P.N. Anderson, R.A. Hitesoh, *Environ. Sci. Technol.* 30 (1996) 1756–1763.

[57] G.V. Buxton, C.L. Greenstock, W.P. Helman, A.B. Ross, *J. Phys. Chem. Ref. Data* 17 (1988) 513–886.

[58] X.Y. Yu, Z.C. Bao, J.R. Barker, *J. Phys. Chem. A* 108 (2004) 295–308.

[59] P. Neta, R.E. Huie, A.B. Ross, *J. Phys. Chem. Ref. Data* 17 (1988) 1027–1284.

[60] C.J. Liang, Z.S. Wang, C.J. Bruell, *Chemosphere* 66 (2007) 106–113.

[61] W.W. Brubaker Jr., R.A. Hites, *Environ. Sci. Technol.* 32 (1998) 3913–3918.

[62] G.P. Anipsitakis, D.D. Dionysiou, M.A. Gonzalez, *Environ. Sci. Technol.* 40 (2006) 1000–1007.

[63] W.F. Wüst, R. Köber, O. Schlicker, A. Dahmke, *Environ. Sci. Technol.* 33 (1999) 4304–4309.

[64] G.P. Anipsitakis, D.D. Dionysiou, *Environ. Sci. Technol.* 38 (2004) 3705–3712.

[65] H.Z. Liu, T.A. Bruton, W. Li, J.V. Buren, C. Prasse, F.M. Doyle, D.L. Sedlak, *Environ. Sci. Technol.* 50 (2016) 890–898.

[66] X. Liang, S. Zhu, Y. Zhong, J. Zhu, P. Yuan, H. He, J. Zhang, *Appl. Catal. B: Environ.* 97 (2010) 151–159.

[67] X. Liang, Y. Zhong, S. Zhu, J. Zhu, P. Yuan, H. He, J. Zhang, *J. Hazard. Mater.* 181 (2010) 112–120.